

DEVELOPMENT OF AN ANTHROPOMORPHIC ROBOT FINGER: MECHANICAL AND KINEMATIC ASPECTS

N. Mifsud
University of Malta
Malta

A. M. Grech
University of Malta
Malta

M. A. Saliba
University of Malta
Malta

S. G. Fabri
University of Malta
Malta

Speaker and Contact Person: M. A. Saliba, Dept. of Manufacturing Engineering, University of Malta, Malta
Email: michael.saliba@um.edu.mt

Topic: Components and Technologies

Keywords: dexterous robot hands; grasping; manipulation

Abstract – In this work, we report on the mechanical design and development, the kinematic analysis, and the simulation of a new dexterous robot finger. The robot finger design is based on that of the human counterpart in size, mechanical structure, and range of motion, and exhibits four distinct joint motions (one abduction/adduction or yaw motion, and three flexion/extension or pitch motions), as does the human finger. Three miniature DC motors with built-in encoders drive the yaw motion of the finger and the two innermost pitch joints. The finger therefore has three independent degrees of freedom. The outermost pitch joint of the finger is mechanically coupled to the middle joint, and the design allows for the variation of the ratio of angular speed between the two coupled joint motions. The motors are installed on the finger itself and on the adjoining section of palm, and the required torques at the joints are obtained through speed reduction transmission systems. An analytical study of the finger, including forward and inverse kinematics and differential kinematics analyses, static force analysis, and computation of joint velocity profiles for straight-line motion of the fingertip, has been carried out. The results of these analyses have been used to develop the control program for the finger, as well as a versatile simulation tool that can be used to optimise future designs of the finger. The simulation program has been validated by comparison to the results of tests carried out on the prototype finger. The ultimate aim of the work is to produce a dexterous robot hand to be used in a flexible manufacturing environment in industry or as a prosthetic device.

1. Introduction

One of the major tasks in robotics, in situations where flexibility is a primary requirement, is the design of the end effector. A biological counterpart of the end effector, the human hand, has a size and dexterity that make it one of the most versatile tools in existence. If it could be reproduced artificially and mounted on robots, the human hand would yield exceptional performance in flexible manufacturing environments. Complemented by appropriate programming and control, this artificial hand would provide an ability to reproduce human operations in hazardous environments, reduce set up times and reduce the need for specialized tools.

Various studies have been carried out on the human hand in order to evaluate its properties and performance from an engineering perspective. In [1], [2], and [3] the average dimensions of the hand were estimated by taking measurements over samples of human subjects. In [4] a study was carried out to model the motion constraints of the human hand, and in particular the ranges of motion of each of the finger joints. The degrees of coupling that exist between the various joints of the hand were described and estimated. In [5], an experimental determination of human grasping forces was carried out using custom-built force sensing devices that were worn over the fingertips during grasping.

The results of studies such as the ones described above have been applied towards the design of artificial hands. Indeed, the development of dexterous fingers and hands has become an active research area in many institutions all over the world. Finger joint actuation has classically been achieved either by using remotely located actuators and tendon transmission systems (e.g. [6], [7]), or by using motors that are located within the finger structure itself (e.g. [8], [9]). More novel approaches have involved the development of a single-piece finger structure [10] and the use of ultrasonic motors to actuate the finger joints [11].

The fingers of the recently developed HIT/DLR hand [12] use brushless DC motors that are located within the linkage structure to actuate the joints. The yaw and pitch motions of the knuckle joint of each finger are achieved using two motors via a bevel gear differential transmission system (this method was also used on the predecessor to this hand [13]), while the pitch motion of the middle joint is achieved through a third motor. The outermost joint of each finger is not actuated independently, but is coupled instead to the corresponding middle joint by means of a rigid linkage.

One of the main objectives of robots is to replace, and often to mimic, human performance in specific environments. The objective of this work is to develop a robot finger that attempts to reproduce the kinematic properties of the human finger.

This work will be applied to the development of a human-scale anthropomorphic robot hand for a wide range of applications, including manufacturing and prosthesis.

2. Design Considerations

Before the actual design process could be started, various aspects had to be considered. This helped to define targets with which the design had to comply.

One of the aspects considered was the size and weight of the robotic finger. The robotic finger was designed to have a size comparable to that of an average adult male. This is required in order to make it easier to implement the robotic finger in a prosthetic device in the future. Another reason is that it would facilitate the use of the finger in conjunction with standard devices e.g. handles, tools. The weight of the robotic finger was also kept as low as possible. Minimizing the weight would increase the payload of the eventual robot hand. Also the lighter the finger, the lighter would be the prosthetic device and hence it would be more attractive to amputees.

Another important aspect to be considered is the maximum force that the robotic finger has to withstand at the fingertip. The results obtained in [5] were used as a guideline for the maximum force exerted at the fingertip of the designed finger.

The robotic finger was designed keeping in mind the bio-mimetic philosophy. In this philosophy, biology is used as the main source of inspiration. In this respect, the robotic finger was designed having four joints. The three outer links represent the proximal phalange, intermediate phalange and distal phalange of the human finger. Having determined the number of joints, the next step is that of determining the number of independent degrees of freedom. Increasing the number of degrees of freedom of the robotic finger would eventually increase the dexterity, at the cost of an increase in the complexity of the control system. A compromise had to be reached between the two and the decision taken was that of designing the robotic finger with three degrees of freedom. Two degrees of freedom would represent flexion and extension movements while a separate degree of freedom would represent abduction and adduction movements. In the human finger, the joints having a flexion and extension movement (pitch movement) are the metacarpal-interphalangeal (MCP) joint, the proximal interphalangeal (PIP) joint, and the distal interphalangeal (DIP) joint. The joint that provides abduction and adduction movements (yaw movement) is the MCP joint. In the human finger the distal phalange cannot be moved unless the intermediate phalange is moved, i.e. the PIP and DIP joints exhibit coupled motion. In our design, we adopted the same approach. The outer joint (equivalent to the DIP joint) is not actuated independently, but is instead coupled to the middle joint (equivalent to the PIP joint).

The kinematic model adopted for the robot finger design is given in Fig. 1, where the joints have been labeled according to their human counterparts. As shown in the figure, the two degrees of freedom of the human MCP joint are replaced by two separate joints, designated MCP1 (for yaw motion) and MCP2 (for flexion/extension or pitch). The displacement constraints of the joints are similar to those of the human being [4]. These are

$$\begin{aligned} -15^{\circ} &\leq \theta_{MCP1} \leq 15^{\circ} \\ 0^{\circ} &\leq \theta_{MCP2} \leq 90^{\circ} \\ 0^{\circ} &\leq \theta_{PIP} \leq 110^{\circ} \\ 0^{\circ} &\leq \theta_{DIP} \leq 90^{\circ} \end{aligned}$$

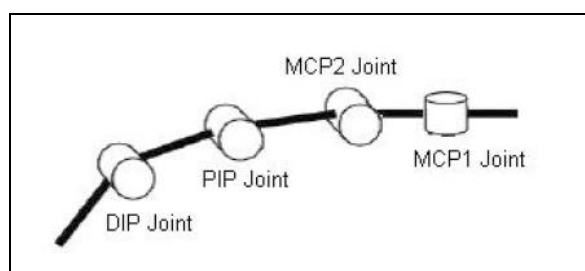


Figure 1 – Structure of the Robot Finger

The robotic finger follows an exoskeleton design, with a rigid outer shell serving as a housing for the actuators and the position sensors required for the control system. In this respect, the design concept is different from that of the human finger, which is based on an endoskeleton design. The reason for this deviation was that in our design, we required to mount the actuators on the finger (and on a section of the palm) itself, in order to have a self-contained unit. It is to be noted that

the human finger does not exhibit this feature, since many of the muscles that actuate the finger joints are located remotely on the forearm.

For an actuation system to be considered suitable for the robotic finger it must be compact, but at the same time it must be able to provide the necessary torque at the finger joint. In this design, use was made of permanent magnet DC motors from maxon motors [14] as actuators. This type of actuator, having a compact and a reasonable cost, is not able to give a high output torque at the shaft. Torque values for such actuators are in the range of mNm. The actuation system, in order to be suitable for the robotic finger, must be able to provide a maximum torque value of around 1.75Nm, which is considerably different from the output torque of the available actuators. Hence in this case a suitable transmission system had to be designed to increase the value of the torque obtained from the actuator. Gears were adopted for speed reduction and eventual increase in output torque. Although gears are complicated in design, they are readily available, reliable in operation and relatively low in cost.

Another important aspect considered during the design stage of the robotic finger was material selection. The materials considered suitable for the main structure of the finger were glycol-modified polyethylene terephthalate (PETG) and polymethyl methacrylate (Perspex). Perspex was the preferred option due to its lower cost, and its availability in a wider range of suitable sheet thicknesses. Perspex also has an exceptionally low value for the specific density, this being only 1.17g/cm^3 , and this helped to reduce the overall weight of the robotic finger. Another advantageous property of Perspex is that it has a good degree of compatibility with the human tissue and thus makes it ideal for prosthetic devices. Since the current model was built for demonstration purposes the optical properties of Perspex (i.e. the fact that it is transparent) was another advantage. Perspex is also easy to machine. For these reasons, the main structure of the robotic finger was constructed using sheets of Perspex. For certain small parts, such as the distal phalanges and the shafts, which required high strength, aluminium was used. Aluminium has a specific density of 2.7g/cm^3 and has a high strength to weight ratio. Aluminium has also good yield strength properties and machinability.

Design for Manufacture (DFM) principles were adopted in the development of the dexterous robotic finger. For example, machining time was reduced by avoiding the use of circlips, which would have required the machining of grooves. Another area where DFM principles were adopted was in the mechanical stops that were designed on the intermediate phalange. The designed mechanical stops were an integral part of the intermediate phalange, and this reduced the need for machining multiple parts and fastening them together. The thickness of the mechanical stops was kept equal to the thickness of the link itself to reduce machining time due to the extra thickness of the mechanical stop. An exploded view of the finger design is shown in Fig.2.

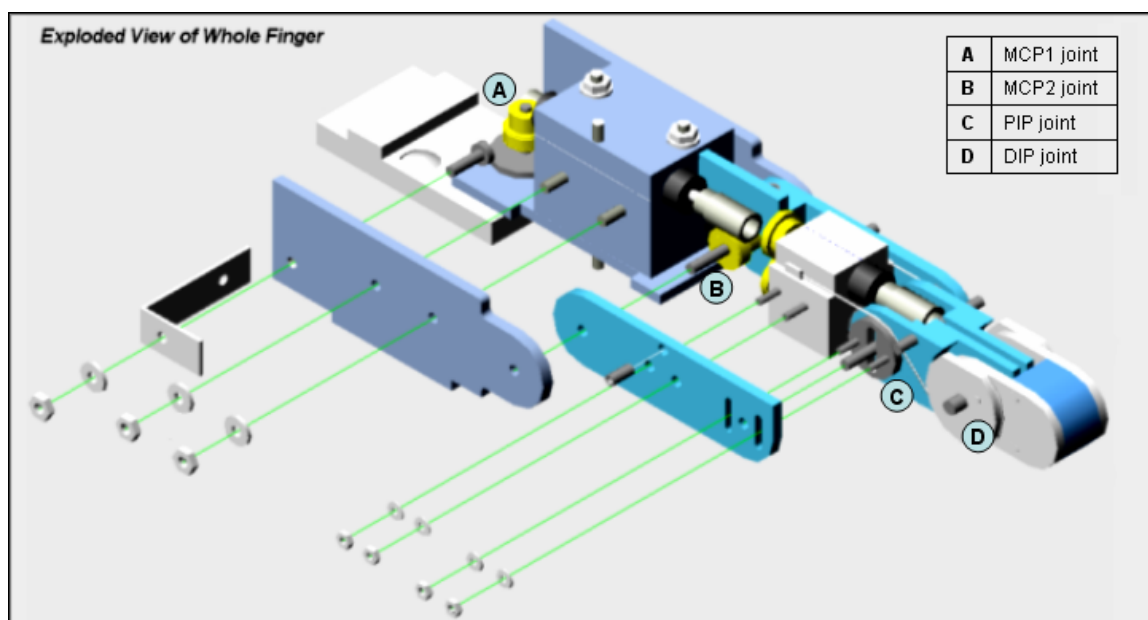


Figure 2 - Intermediate Phalange after applying DFM Guidelines

Design for assembly (DFA) techniques were also adopted in this work. For example, in the design of the actuator housing, the solution adopted involved that of stacking the actuators on top of each other, thus achieving a 'sandwich effect', which rigidly retained the actuators. The assembly of the actuators is shown in Fig.3.

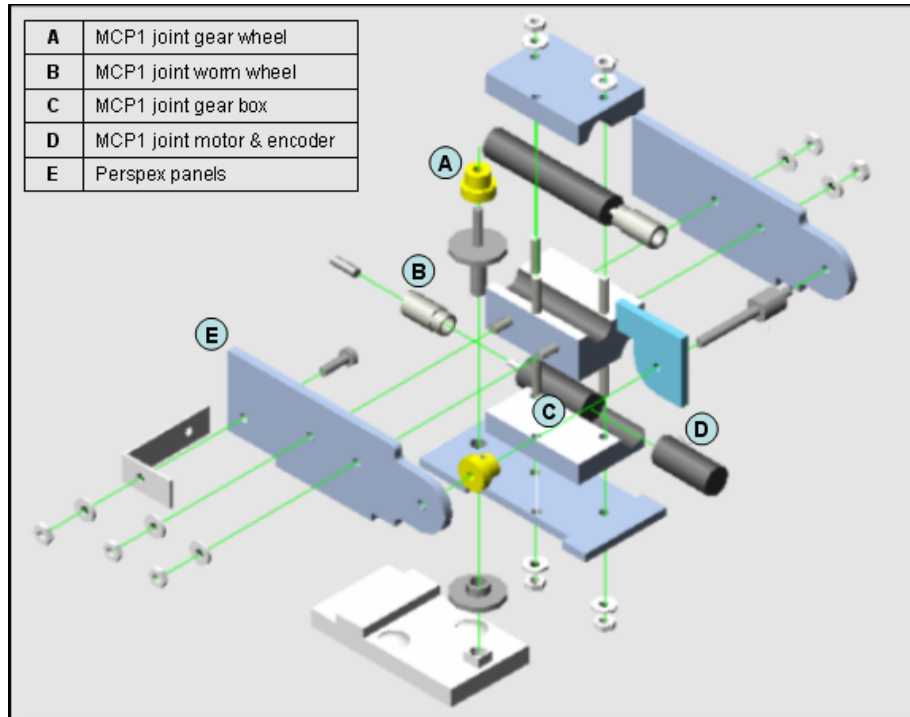


Figure 3 - Assembly of Actuators in Palm

The robotic finger was also designed to be modular. An example of this is the fingertip design, which was itself modular (Fig.4). The tip can be modified according to the specific application of the robotic finger, and could for example be equipped with a slip or tactile sensor if required.

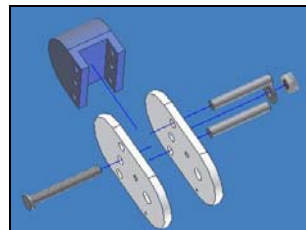


Figure 4 - Assembly of Fingertip to the Distal Phalanges

3. Mechanical Design of the Finger

The robotic finger was designed using the dimensions listed in Table 1.

Distal Phalange Length	30mm
Intermediate Phalange Length	30mm
Proximal Phalange Length	55mm
Robotic Finger Length	115mm
Finger Thickness	20mm
Maximum Finger Breadth	32mm
Minimum Finger Breadth	19mm
Palm Length	80mm

Table 1 - Dimensions of the Robotic Finger

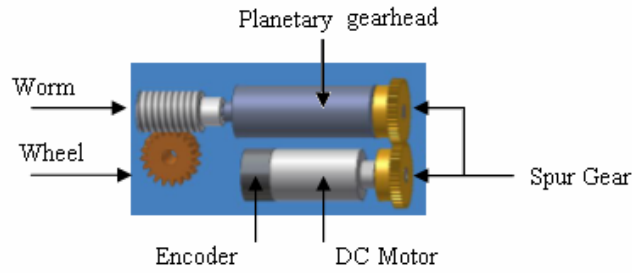


Figure 5 - Mechanism mounted in the Proximal Phalange

The mechanism mounted in the proximal phalange is quite compact and weighs only 24.6g (refer to Fig.5). The mechanism consists of a 0.75W DC motor, two spur gears, a planetary gear head, and a single thread worm and wheel. In usual design set-ups, the shaft of the motor serves as a direct input to the planetary gear head. In this case, due to space constraints, a suitable flange at the gear head input was designed and two spur gears with gear ratios 1:1 were used. The planetary gear head chosen has a reduction ratio of 1024:1. The actual torque value at the PIP Joint is 1Nm, which is comparable to the torque value available on the human counterpart.

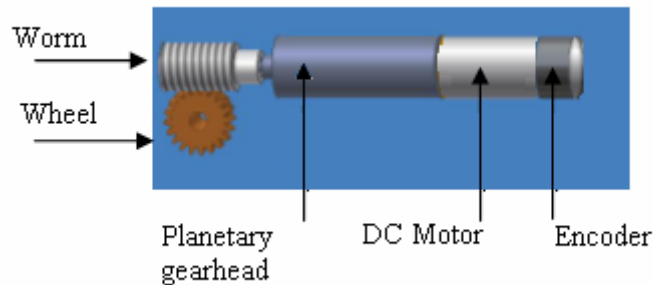


Figure 6 - Mechanism mounted in the Palm

The mechanism that actuates the proximal phalange is mounted in the palm and is illustrated in Fig.6.

Besides having flexion and extension movements, the robotic finger exhibits also abduction and adduction movements. The output torque requirement is similar to that of the pitch mechanism mounted in the proximal phalange. Hence it was possible to use the same mechanism as shown in Fig.6 with some modifications. The yaw mechanism at the MCP1 joint is shown in Fig.7.

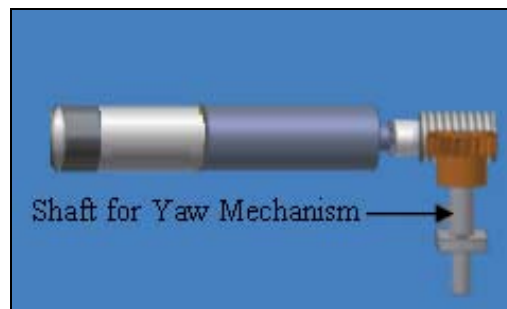


Figure 7 - Yaw Mechanism

The coupling mechanism adopted for the two outer links was designed based on the constraints established by Lin et al [4]. The relationship between the two joints was therefore defined to be:

$$\theta_{DIP} = \frac{2}{3}\theta_{PIP}$$

where θ_{DIP} represents the flexion angle of the DIP joint and θ_{PIP} represents the flexion angle of the PIP joint. The above

relationship was achieved using a cable system. Although the cable system is simple and has various advantages, it only works in one direction. This meant that a suitable return mechanism also had to be designed. The return mechanism adopted is one involving springs.

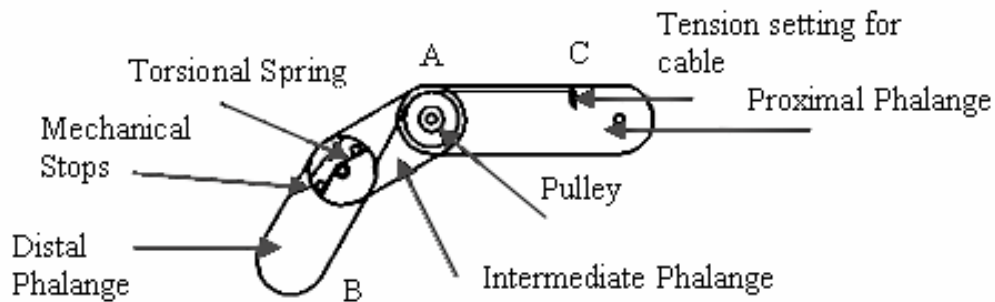


Figure 8 - Cable Mechanism for the Distal Phalange

The coupled mechanism is shown in Fig.8 and consists of a cable, which is connected to the distal phalange, passed over a pulley at the PIP joint and finally rigidly affixed to the proximal phalange. A nut lock system is used to retain the cable in position at point C. This will also serve to give the cable the required tension. As the intermediate phalange rotates, the cable is wound around pulley A and unwound from pulley B. When the distal phalange rotates, potential energy is stored in the torsional spring, which will eventually be used to return the distal phalange back to the initial position. In this way the relationship between θ_{PIP} and θ_{DIP} depends on the ratio of the radii of the pulleys A and B. Different relationships between θ_{PIP} and θ_{DIP} were achievable by implementing a mechanism whereby the position of pulley A could be adjusted in a vertical plane.

The shaft of each DC motor is coupled to an incremental encoder having a resolution of 256 pulses per motor shaft revolution. The encoder signals are connected to the control system from which joint angle can be calculated, providing positional feedback information. The joint angle controller is implemented digitally on a desktop PC via an input-output interface board. The interface board reads the encoder signals and also generates reference signals to the current driver circuits actuating the motors. Communication of signals between the interface board and the three motor/encoder pairs takes place on a time-multiplexed basis. The control program, coded in C language, implements a pole-placement control algorithm with integral action for every motor.

At start up the incremental encoders need to be reset at a predefined angular position, this is done by moving all the joints counter-clockwise until the current driver circuits indicate that they have hit mechanical stops. The program then resets the variables associated with the angular position values of the motors.

The designed dexterous robotic finger and the actual prototype are shown in Fig.9 and Fig.10 respectively.

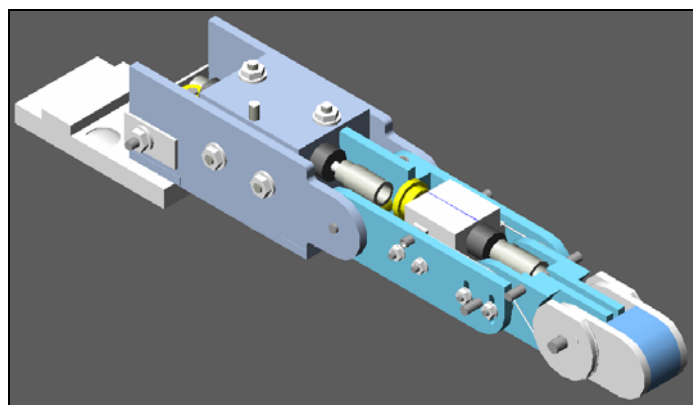


Figure 9 – CAD drawing of the Robotic Finger (Autodesk Inventor®)

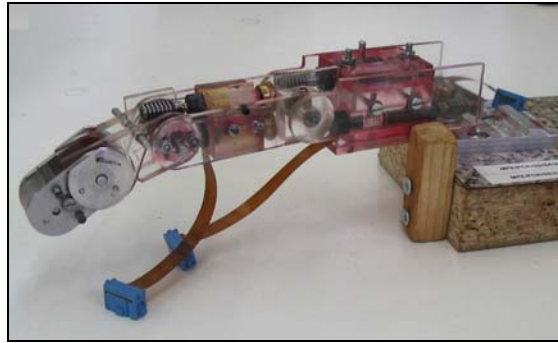


Figure 10 - Prototype Robotic Finger

4. Kinematic & Static Force Analysis of the Finger

General

The Kinematics of the finger describes the relationship between the joint angles and the position/orientation of the fingertip. It involves the solution of both the Direct Kinematics and Inverse Kinematics problems. In our application, the results of the analysis were used to develop the control program for the finger, and later to develop a simulation program. The Denavit-Hartenberg (DH) convention was used to develop the analysis of the kinematics of the robot finger. The local reference frames used to give the relation between the fingertip and the fixed reference frame in terms of joint variables, are shown in Fig.11.

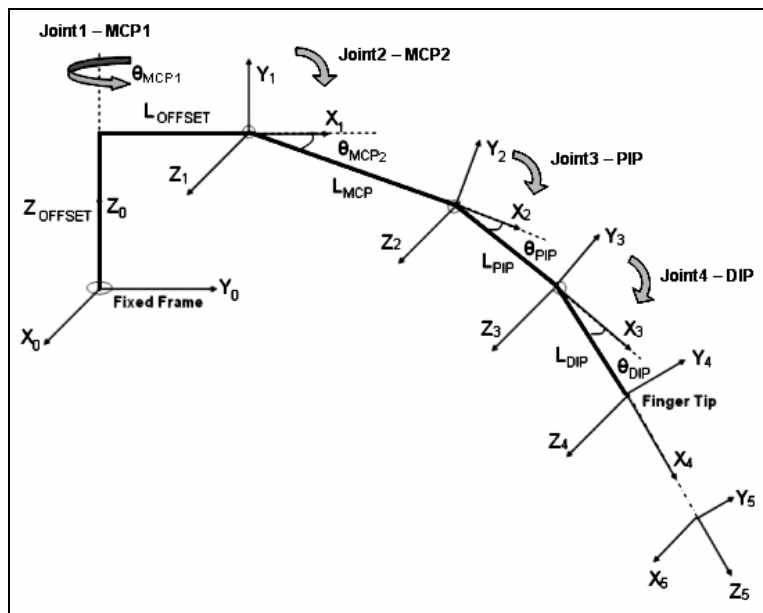


Figure 11 - Reference Frames at Joints

The pulley mechanism at the PIP joint, which is used to move the PIP and DIP joints at a specified ratio, may be adjusted to be off-centre either upwards or downwards. A detailed analysis using geometric methods was carried out to derive the relation between the PIP to DIP joint ratio and the pulley eccentric shift. The results are shown in Fig.12. This analysis showed that the relation between the DIP joint angle and the PIP joint angle becomes slightly non-linear when the centre of the pulley is shifted either upwards or downwards. The relationship between the two joint motions, however, could still be approximated to a linear one over a large part of the range of motion of the finger. The ratio R_{DP} is given by

$$R_{DP} = \theta_{DIP} / \theta_{PIP}$$

By using the adjustable pulley mechanism, R_{DP} could be varied between the approximate limits of 0.5 and 0.8.

Normal robotic structures are designed not to have more than two links connected consecutively in parallel to avoid redundancies and hence simplify the calculations. The finger has three consecutive links connected in parallel, but since two of them, i.e. the DIP and PIP joints are dependent on each other, the redundancy is eliminated. The use of three links instead of two facilitates the grasping process.

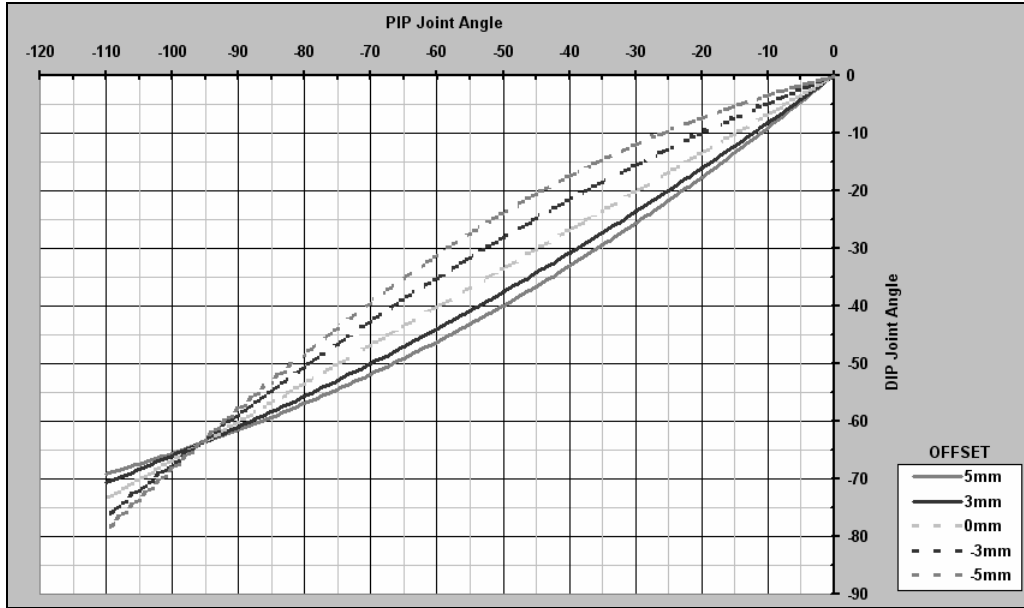


Figure 12 - PIP to DIP Ratio Plot at Various Shift Values

Forward Kinematics

The equations for the fingertip position as derived using the DH convention are given by

$$\begin{aligned} P_X &= \cos\theta_{MCP1} (L_{DIP} \cos\theta_A + L_{PIP} \cos\theta_B + L_{MCP} \cos\theta_{MCP2} + L_{Offset}) \\ P_Y &= \sin\theta_{MCP1} (L_{DIP} \cos\theta_A + L_{PIP} \cos\theta_B + L_{MCP} \cos\theta_{MCP2} + L_{Offset}) \\ P_Z &= L_{DIP} \sin\theta_A + L_{PIP} \sin\theta_B + L_{MCP} \sin\theta_{MCP2} + Z_{Offset} \end{aligned}$$

where (P_X, P_Y, P_Z) are the coordinates of the fingertip in the fixed reference frame; $\theta_A = (\theta_{MCP2} + \theta_{PIP} (1 + R_{DP}))$; $\theta_B = (\theta_{MCP2} + \theta_{PIP})$; and the remaining parameters are defined in Fig.11.

Inverse Kinematics

The Inverse Kinematics solution gives the angular positions of the joints as functions of the fingertip position in the workspace. The geometric approach was chosen to calculate the inverse kinematics, and an iterative technique was used to compute the required joint positions. The permitted ranges of the coordinates of the fingertip (shown below) were included in the control program to keep the iteration loop in the permissible range:

$$P_X \leq L_{TIPmax}$$

where L_{TIPmax} is the length between the axis of the MCP1 joint and the fingertip of the fully extended finger

$$L_{TIPmax} \sin(-15^\circ) \leq P_Y \leq L_{TIPmax} \sin(15^\circ)$$

due to the mechanical constraints of the MCP1 joint, set to be $-15^\circ \leq \theta_{MCP1} \leq 15^\circ$ based on Lin et al [4].

$$(Z_{Offset} - (L_{MCP} + L_{PIP} + L_{DIP})) \leq P_Z \leq Z_{Offset}$$

due to the mechanical constraints of the flexion/extension joints.

The values for the other variables must be in the range

$$L_{TIP} \leq L_{TIPmax}$$

$$0 \leq L_{MT} \leq (L_{MCP} + L_{PIP} + L_{DIP})$$

$$L_{PT} \leq (L_{PIP} + L_{DIP})$$

where L_{MT} is the distance between the MCP2 joint axis and fingertip, and L_{PT} is the distance between the PIP joint axis and finger tip (see Fig. 13).

In the first part the control program prompts the user for the desired position of the fingertip and for the pulley offset values. After confirming that the values inputted are in the permissible range, the maximum possible MCP2 joint angle θ_{MCP2} to the line L_{MT} (Fig.13) is computed by

$$\theta_{MCP2max} = \text{Sin}^{-1} ((L_{Offset} - P_z) / L_{MT})$$

for $(L_{TIP} - L_{Offset}) \geq 0$

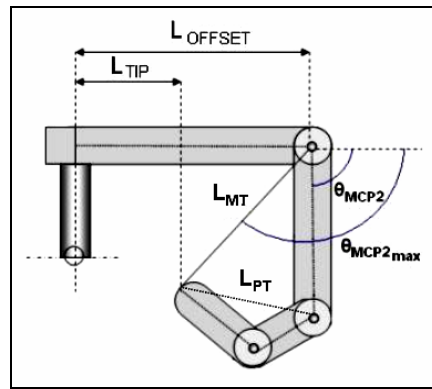


Figure 13 - $\theta_{MCP2max}$ for Start of Iteration Loop

but if $(L_{TIP} - L_{Offset}) < 0$ as shown in Fig.13, then the maximum possible MCP2 joint angle $\theta_{MCP2max}$ must be equal to 90° , due to the constraint $0^\circ \leq \theta_{MCP2} \leq 90^\circ$ [4].

The C-program starts from $\theta_{MCP2max}$ as a fixed angle and computes the forward kinematic equations, for $0^\circ \leq \theta_{PIP} \leq 90^\circ$ at a predefined increment iteratively. The MCP2 angle is then decreased by a predefined decrement and the iteration for θ_{PIP} is repeated until the constraint $R_{DP} = \theta_{DIP} / \theta_{PIP}$ is satisfied within a prespecified tolerance. If $\theta_{MCP2max}$ is decreased to a value less than 0° the program stops and informs the user that no solution was found. Fig.14 shows the flowchart for the inverse kinematics compilation.

Differential Kinematics

Differential Kinematics gives the relationship between the joint angular velocity $\dot{\theta}$ and the fingertip in terms of velocities \dot{p} along the fixed reference axes. Since the finger has four joints but three degrees of freedom, the Jacobian matrix was not a square matrix.

The Jacobian matrix of the finger is:

$$\bar{J} = \begin{bmatrix} J_{P11} & J_{P12} & J_{P13} & J_{P14} \\ J_{P21} & J_{P22} & J_{P23} & J_{P24} \\ J_{P31} & J_{P32} & J_{P33} & J_{P34} \\ \begin{bmatrix} 0 & s\theta_{MCP1} & s\theta_{MCP1} & s\theta_{MCP1} \\ 0 & -c\theta_{MCP1} & -c\theta_{MCP1} & -c\theta_{MCP1} \\ 1 & 0 & 0 & 0 \end{bmatrix} \end{bmatrix}$$

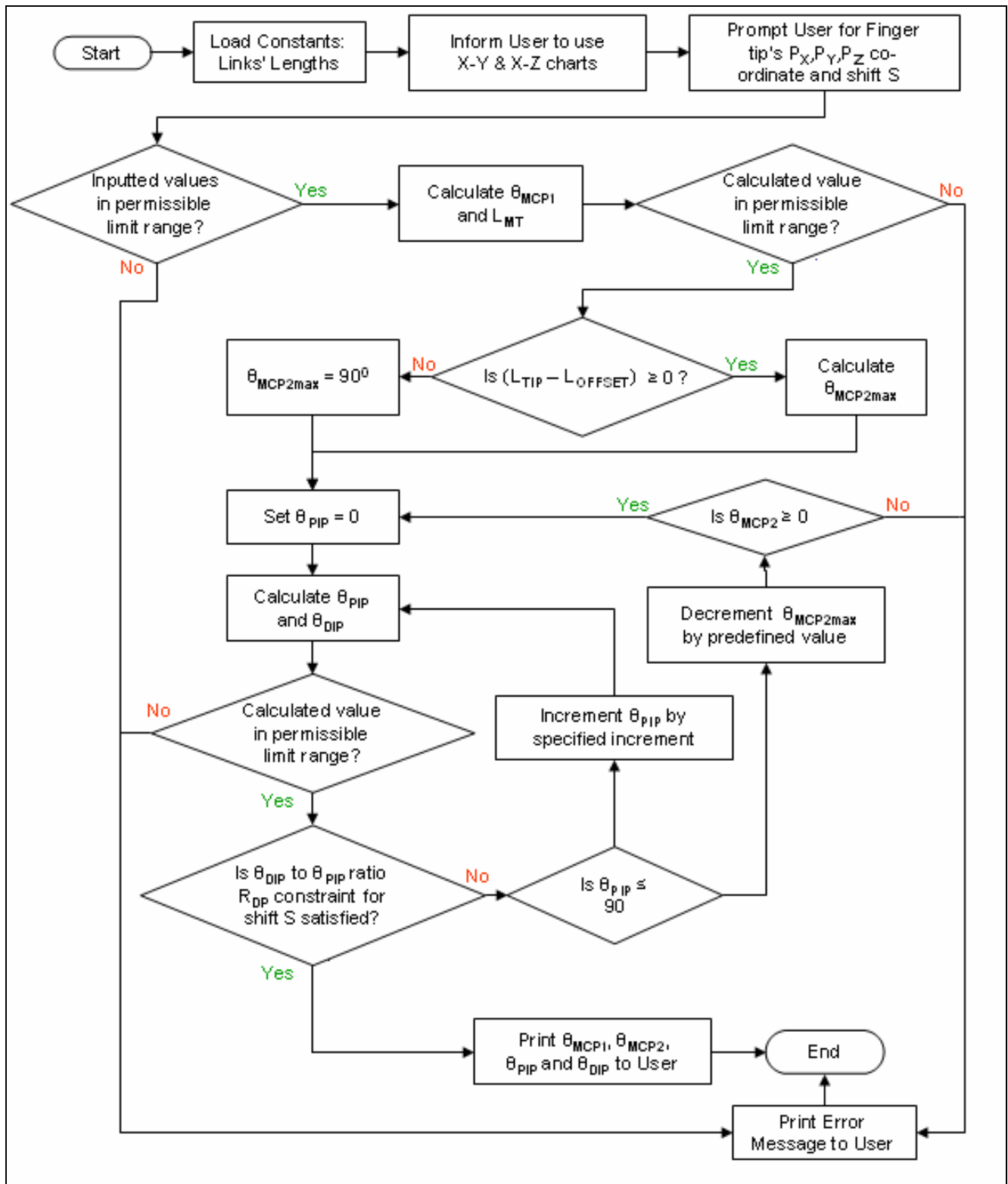


Figure 14 - Inverse Kinematics Program Flowchart

where:

$$J_{P_{11}} = -S\theta_{MCP1} (L_{DIP}C\theta_A + L_{PIP}C\theta_B + L_{MCP2}C\theta_{MCP2} + L_{Offset})$$

$$J_{P_{21}} = C\theta_{MCP1} (L_{DIP}C\theta_A + L_{PIP}C\theta_B + L_{MCP2}C\theta_{MCP2} + L_{Offset})$$

$$J_{P_{31}} = 0$$

$$J_{P_{12}} = -C\theta_{MCP1} (L_{DIP}S\theta_A + L_{PIP}S\theta_B + L_{MCP2}S\theta_{MCP2})$$

$$J_{P_{22}} = -S\theta_{MCP1} (L_{DIP}S\theta_A + L_{PIP}S\theta_B + L_{MCP2}S\theta_{MCP2})$$

$$J_{P_{32}} = (L_{DIP}C\theta_A + L_{PIP}C\theta_B + L_{MCP2}C\theta_{MCP2})$$

$$J_{P_{13}} = -C\theta_{MCP1} (L_{DIP}S\theta_A + L_{PIP}S\theta_B)$$

$$J_{P_{23}} = -S\theta_{MCP1} (L_{DIP}S\theta_A + L_{PIP}S\theta_B)$$

$$J_{P_{33}} = (L_{DIP}C\theta_A + L_{PIP}C\theta_B)$$

$$J_{P_{14}} = -C\theta_{MCP1} (L_{DIP}S\theta_A)$$

$$J_{P_{24}} = -S\theta_{MCP1} (L_{DIP}S\theta_A)$$

$$J_{P_{34}} = (L_{DIP}C\theta_A)$$

and $C\theta \equiv \cos \theta$, $S\theta \equiv \sin \theta$

The linear velocities of the fingertip along the x , y and z -axes are given by:

$$\dot{P}_{X_0} = \dot{\theta}_{MCP1}J_{P_{11}} + \dot{\theta}_{MCP2}J_{P_{12}} + \dot{\theta}_{PIP} (J_{P_{13}} + R_{DP}J_{P_{14}})$$

$$\dot{P}_{Y_0} = \dot{\theta}_{MCP1}J_{P_{21}} + \dot{\theta}_{MCP2}J_{P_{22}} + \dot{\theta}_{PIP} (J_{P_{23}} + R_{DP}J_{P_{24}})$$

$$\dot{P}_{Z_0} = \dot{\theta}_{MCP2}J_{P_{32}} + \dot{\theta}_{PIP} (J_{P_{33}} + R_{DP}J_{P_{34}})$$

where $\dot{\theta}_{MCP1}$, $\dot{\theta}_{MCP2}$ and $\dot{\theta}_{PIP}$ are the angular velocities of the MCP1 (abduction/adduction), MCP2 (flexion) and PIP joints respectively; and $J_{P_{ij}}$ is the term taken from row i and column j of the positional Jacobian matrix.

A closed form for the Inverse Differential Kinematics solution was obtained by solving the Forward Differential Kinematics and the PIP to DIP ratio constraint simultaneously. The following solutions were obtained for each joint:

$$\dot{\theta}_{MCP2} = \frac{J_{P_{11}}\dot{P}_{Y_0} - J_{P_{21}}\dot{P}_{X_0} + \dot{P}_{Z_0} \left(\frac{J_{P_{21}}(J_{P_{13}} + R_{DP}J_{P_{14}}) - J_{P_{11}}(J_{P_{23}} + R_{DP}J_{P_{24}})}{(J_{P_{33}} + R_{DP}J_{P_{34}})} \right)}{J_{P_{22}}J_{P_{11}} - J_{P_{12}}J_{P_{21}} + J_{P_{32}} \left(\frac{J_{P_{21}}(J_{P_{13}} + R_{DP}J_{P_{14}}) - J_{P_{11}}(J_{P_{23}} + R_{DP}J_{P_{24}})}{(J_{P_{33}} + R_{DP}J_{P_{34}})} \right)}$$

$$\dot{\theta}_{PIP} = \frac{J_{P_{32}}(\dot{P}_{Y_0}J_{P_{11}} - \dot{P}_{X_0}J_{P_{21}}) + \dot{P}_{Z_0}(J_{P_{12}}J_{P_{21}} - J_{P_{22}}J_{P_{11}})}{\left((J_{P_{33}} + R_{DP}J_{P_{34}})(J_{P_{12}}J_{P_{21}} - J_{P_{22}}J_{P_{11}}) \right) - J_{P_{32}}(J_{P_{21}}(J_{P_{13}} + R_{DP}J_{P_{14}}) + J_{P_{11}}(J_{P_{23}} + R_{DP}J_{P_{24}}))}$$

$$\dot{\theta}_{MCP1} = \frac{\dot{P}_{Y_0} - \dot{\theta}_{MCP2}J_{P_{22}} - \dot{\theta}_{PIP}(J_{P_{23}} + R_{DP}J_{P_{24}})}{J_{P_{21}}}$$

Motion Path Planning

The Kinematics and Differential Kinematics analyses were used for the planning of the joint angles and joint angular velocities required to move the fingertip along a path between the current position and the desired position. This was carried out for two modes of motion, the point-to-point (joint interpolated) mode and the straight-line mode.

Joint interpolated mode:

In joint interpolated mode no constraints are placed on the path followed by the fingertip between the current position and the desired position. The joint angle with the largest required travel is driven at maximum allowable speed whilst the remaining joints are driven with an angular velocity such that all joints start and complete their motion simultaneously.

The joint interpolated method does not need a lot of computational power since the joints travel at a constant speed through the path. The joint angles are obtained from the inverse kinematics solution for both the current position P_C and the destination position P_D of the fingertip. Then for each joint the corresponding angular distance $\Delta\theta$ is obtained by subtracting the appropriate joint angles e.g. $\theta_{PIP_D} - \theta_{PIP_C}$. The largest $\Delta\theta$ from the MCP1, MCP2 and PIP joint angles is moved at the predefined maximum angular velocity ω_{max} . The time t_{max} required for the whole complete motion is calculated and recorded. The other joints are moved at a constant angular velocity, in such a way that all angles start and finish at the same time t_{max} , with

$$t_{max} = \frac{\Delta\theta_{max}}{\omega_{max}}$$

$$\omega_j = \frac{\Delta\theta_j}{t_{max}} \text{ where } j = \text{MCP1, MCP2 and PIP}$$

Straight-line mode:

In straight-line mode, the joint movements are coordinated such that the fingertip travels through a linear path between the current position and the desired position (Fig.15). This makes it an ideal operation when the finger is inserting a pin in a hole or moving along a surface.

The length of linear path is

$$d = \sqrt{(X_D - X_C)^2 + (Y_D - Y_C)^2 + (Z_D - Z_C)^2}$$

where (X_C, Y_C, Z_C) and (X_D, Y_D, Z_D) are the co-ordinates of the finger tip current position and desired position respectively, relative to the reference frame. (See Fig.15)

Resolving the required linear velocity v_L along the path to the axes of the world reference frame:

$$\dot{P}_{x_0} = \left(\frac{v_L (X_D - X_C)}{d} \right)$$

$$\dot{P}_{y_0} = \left(\frac{v_L (Y_D - Y_C)}{d} \right)$$

$$\dot{P}_{z_0} = \left(\frac{v_L (Z_D - Z_C)}{d} \right)$$

The time required for completing motion $t_{total} = \left(\frac{d}{v_L} \right)$

The time required for each increment $t_{inc} = \frac{d_{inc}}{v_L} = \frac{d_{inc}}{d} t_{total}$

where d_{inc} is a predefined length for the increment along the path as shown in Fig.15.

Then for $0 \leq i \leq \left(\frac{d}{d_{inc}} \right)$ the following values for each increment are computed:

$$X_i = \left(X_C + \frac{id_{inc}}{d} (X_D - X_C) \right)$$

$$Y_i = \left(Y_C + \frac{id_{inc}}{d} (Y_D - Y_C) \right)$$

$$Z_i = \left(Z_C + \frac{id_{inc}}{d} (Z_D - Z_C) \right)$$

The smaller the increments are ($d_{inc} \rightarrow 0$), the better is the motion along the path, but the more computational power and memory are required. For the list of points produced the inverse kinematics and inverse differential kinematics are calculated. Then the finger is set to move from each point to each consecutive point at the respective calculated angular velocities. It is important to note that, in the application of this analysis for simulation purposes none of the joints must be allowed to move at a velocity higher than a preset maximum limit.

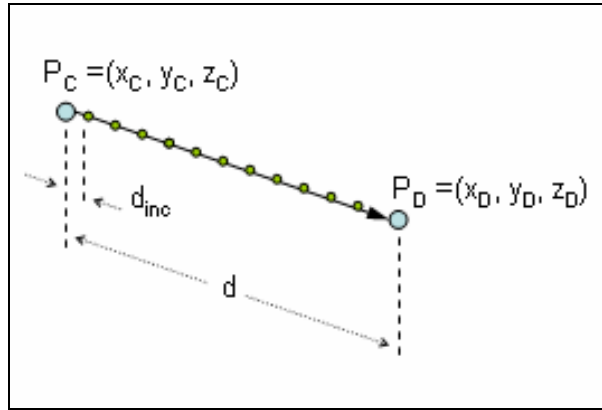


Figure 15 - Linear Motion of the Fingertip

The flowchart for the structure of the trajectory planning is shown in Fig.16. An example of the velocity profile for each joint for a straight-line path is shown in Fig.17.

Static Forces

The Jacobian matrix was used to determine the relation between the forces at the fingertip along the fixed reference frame axes and the torques applied at the joints when in static equilibrium configuration. The statics model is represented by the following equation

$$\tau = \bar{J}^T \gamma$$

where τ is the matrix representing the torque at each joint and γ is the matrix representing the forces at the fingertip along each respective axis. The weight W of each link was measured and the centres of gravity were found experimentally. From this the contribution to the joints' torques by the links' weights could be calculated and added to derived equations in the static model.

The contribution of the weight W of the links along the Z-axis, which is taken to act at the centre of gravity κ of each joint is given by:

$$\tau_{ZG_{MCP}} = W_{MCP} \kappa_{MCP} C\theta_{MCP} + W_{PIP} (L_{MCP} C\theta_{MCP} + \kappa_{PIP} C\theta_B) + W_{DIP} (L_{MCP} C\theta_{MCP} + L_{PIP} C\theta_B + \kappa_{DIP} C\theta_A)$$

$$\tau_{ZG_{PIP}} = W_{PIP} (\kappa_{PIP} C\theta_B) + W_{DIP} (L_{PIP} C\theta_B + \kappa_{DIP} C\theta_A)$$

$$\tau_{ZG_{DIP}} = W_{DIP} (\kappa_{DIP} C\theta_A)$$

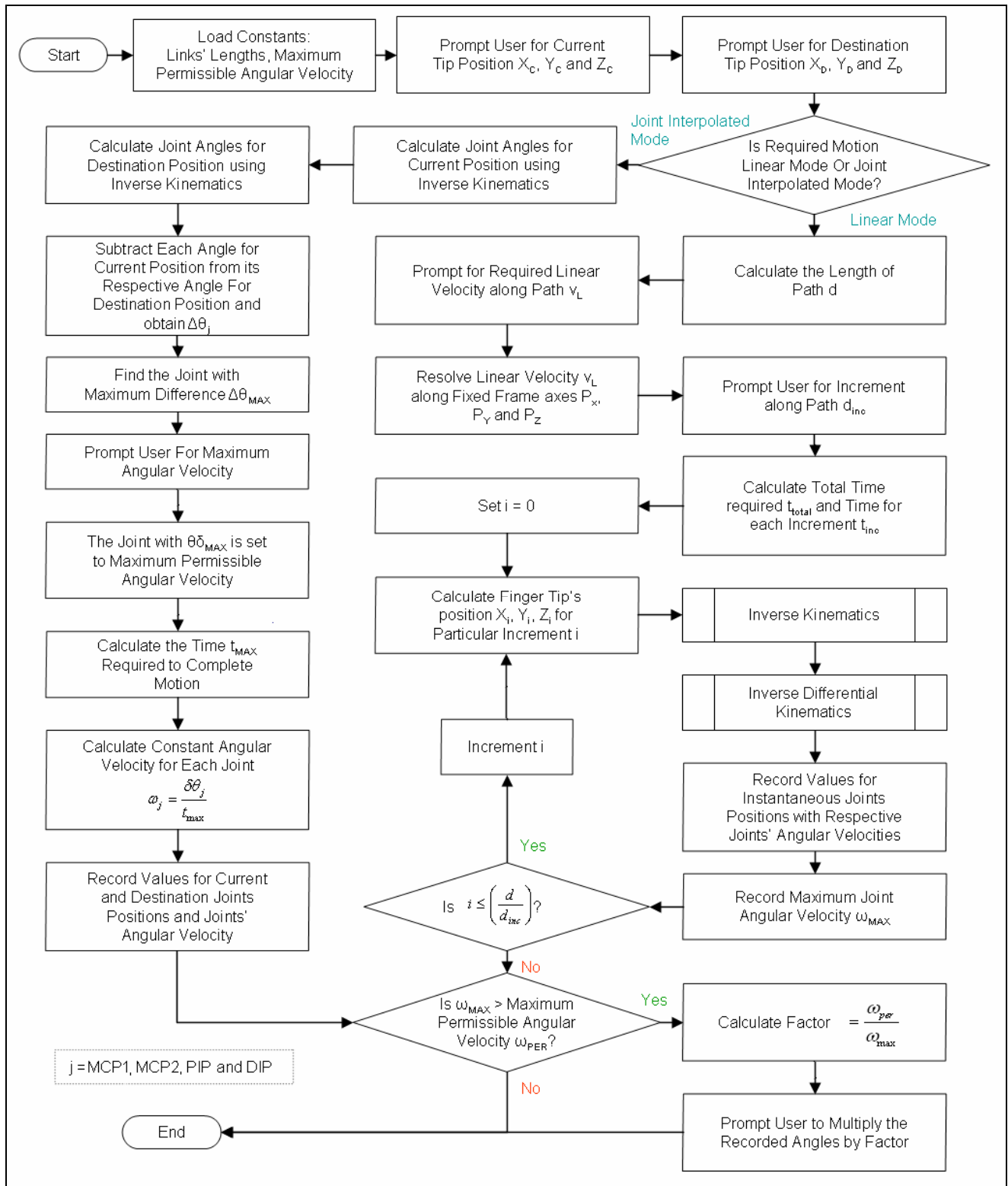


Figure 16 - Motion Path Planning Simulation Program Flowchart

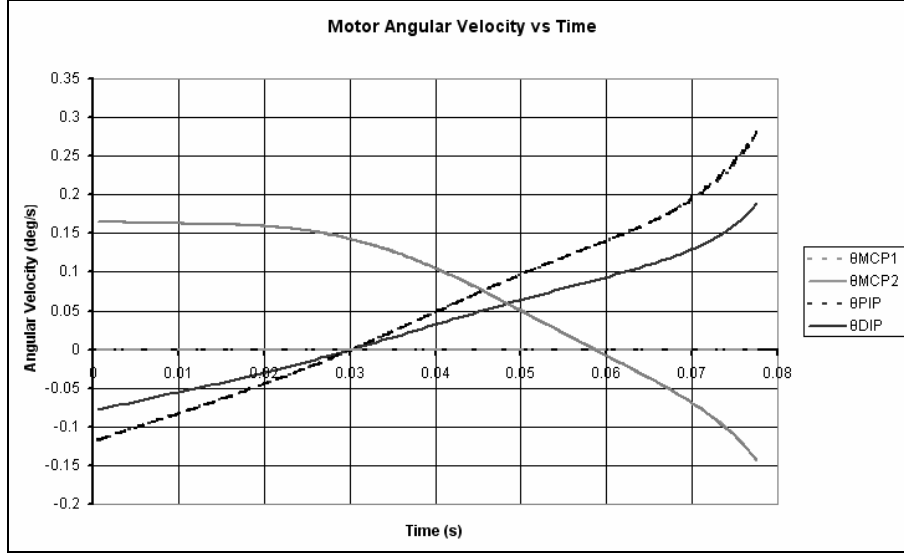


Figure 17 - Angular Velocities Obtained for a Linear Motion Mode

The force f at the fingertip for the known motor joint torques τ_{Motor} is given by:

$$f_X = \frac{J_{P_{21}} \left(J_{P_{33}} (\tau_{MotorMCP2} - \tau_{ZG_{MCP}}) - J_{P_{32}} (\tau_{MotorPIP} - (\tau_{ZG_{PIP}} + \tau_{RS})) \right) - \tau_{MotorMCP1} (J_{P_{33}} J_{P_{22}} - J_{P_{23}} J_{P_{32}})}{J_{P_{21}} (J_{P_{33}} J_{P_{12}} - J_{P_{13}} J_{P_{32}}) - J_{P_{11}} (J_{P_{33}} J_{P_{22}} - J_{P_{23}} J_{P_{32}})}$$

$$f_Y = \frac{J_{P_{11}} \left(J_{P_{33}} (\tau_{MotorMCP2} - \tau_{ZG_{MCP}}) - J_{P_{32}} (\tau_{MotorPIP} - (\tau_{ZG_{PIP}} + \tau_{RS})) \right) - \tau_{MotorMCP1} (J_{P_{33}} J_{P_{12}} - J_{P_{13}} J_{P_{32}})}{J_{P_{11}} (J_{P_{33}} J_{P_{22}} - J_{P_{23}} J_{P_{32}}) - J_{P_{21}} (J_{P_{33}} J_{P_{12}} - J_{P_{13}} J_{P_{32}})}$$

$$f_Z = \frac{\tau_{motorMCP2} - J_{P_{12}} f_X - J_{P_{22}} f_Y}{J_{P_{32}}}$$

where τ_{RS} is the torque experienced on the PIP joint by the return spring at the DIP joint.

5. Simulation of Finger Kinematics

A computer simulation program, based on the results of the kinematic analysis, was developed using the C language. The simulation program includes all the models mentioned, i.e. Kinematics, Differential Kinematics, and Statics as well as reach plotting and workspace volume calculation. Constraints were implemented in the program to avoid singularities, and to avoid variables getting out of the permissible range. The models were used to give the required information to the position control system for the trajectory of the robot finger. The simulation may later be utilised in the conceptual design of a robot finger to achieve specific performance criteria. An animation was also developed to show the posture of the finger during calculation. It is also used to visualise the path of the finger during trajectory planning.

Validation

The validation of the program was done by performing experiments on prototype finger models and comparing the results to the simulation program, checking that values correspond to each other. During programming a consistency check was made, whereby the values obtained by the inverse kinematics and inverse differential kinematics were checked to correspond to the values obtained by forward kinematics and forward differential kinematics respectively.

For kinematics verification the corresponding actual fingertip position in relation to the joint angles was compared to those of the simulation. An actual size cardboard finger model with the corresponding joints was built and attached to a graph

paper (Fig.18). The joints can be moved freely to the desired joint angles. The actual joint angles were entered in the simulation program and the output obtained from kinematics for the fingertip position was checked to correspond to the actual position of the fingertip.

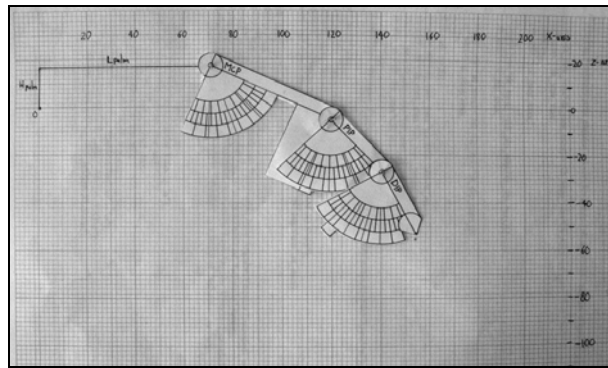


Figure 18 - Prototype for Kinematics Validation

The differential kinematics were validated by moving one joint at a time at constant speed. The joint was moved by a finite but small predefined angle $\Delta\theta$ (as shown in Fig.19) and the time taken t for the complete motion was recorded by the control system. The motion of the fingertip from point C to point D was assumed to be linear, and by measuring the components of the distance along each axis and dividing it by time t , the linear velocity along each axis could be calculated. This was then compared to the values of the fingertip linear velocity obtained in the simulation program for the same joint angular velocity. The distance between the fingertip starting position C and final position D was obtained by the inverse kinematics program from the known joint angles. This validation procedure was carried for all three independently movable joints.

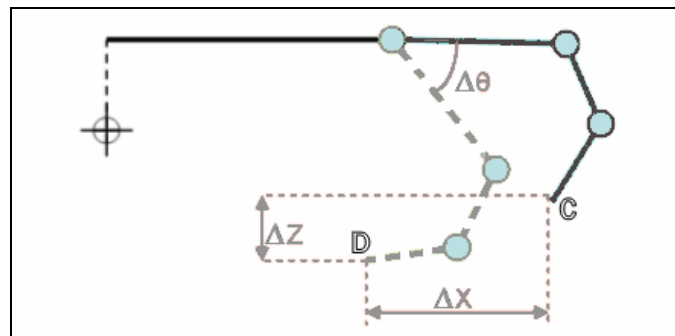


Figure 19 - Differential Kinematics Validation

To validate the statics model the force developed at the fingertip along the fixed reference frame axes was checked to correspond to the actual torque at the motors. The force at the fingertip was calculated by compressing a spring with known spring constant. The torque at each joint was developed by hanging standard masses to a pulley attached to the free joint (Fig.20), each time recording the spring deflection at the finger tip, while keeping the other joints fixed. The experiment was repeated for the MCP1, MCP2 and PIP joints.

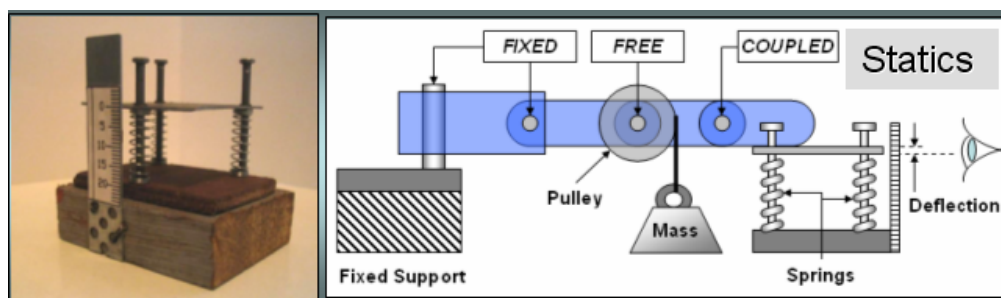


Figure 20 – Springs and Statics Validation Setup

Finger Work Envelope Plotting, Workspace Volume and Area calculation

Using the results of the Kinematics analysis the work envelope of the finger tip along the X-Z and X-Y fixed reference frame axes, with $\theta_{MCP1} = 0$ could be plotted (Fig.21).

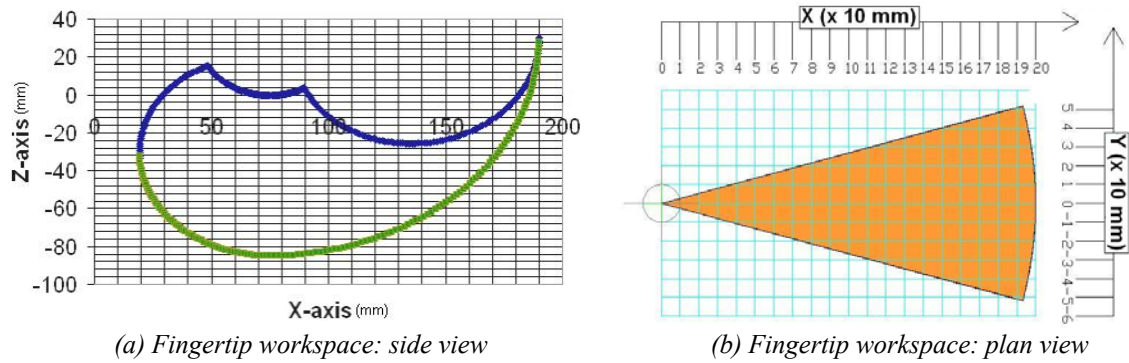


Figure 21 - Locus Plot of Anthropomorphic Robot Finger

This was performed by moving the joints from one extremity to another systematically (Fig.22), each time recording the position of the fingertip by forward kinematics. The work envelope plotting is important in inverse kinematics as it helps the user visualise the region in which the fingertip may be located.

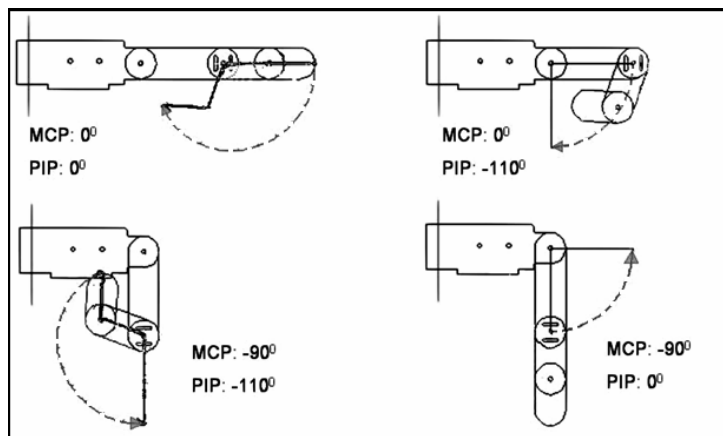


Figure 22 - Finger Motion during Locus Plotting

The program first calculates the volume between the upper dark line in Fig.21 and the highest point Z_{Offset} where Z_{Offset} is the predefined height of the palm above the origin. The program then subtracts this from the volume between the dotted line and the same highest point Z_{Offset} . The equation for the workspace volume is:

$$V = \sum \delta V = \sum \frac{\pi}{24} (x_{i-1}^2 - x_i^2) (2Z_{OFFSET} - z_{L_{i-1}} - z_{L_i})$$

The developed simulation program was utilised to obtain the workspace volume and work envelope area of the robot finger by means of numerical integration. The link lengths for maximum volume and maximum area as fractions of the total finger length L , keeping the palm length constant, are shown in Table 2.

Criteria	Proximal Phalange	Intermediate Phalange	Distal Phalange	Value
Volume _{Max}	0.57L	0.2L	0.23L	4330L ³
Area _{Max}	0.52L	0.21L	0.27L	84L ²

Table 2 – Link lengths for Specific Criteria

It is noted that in Table 2 it was assumed that the links had a thickness added below the links, of similar dimensions as that of a human. The results yielded were similar to those of an anthropomorphic finger.

6. Preliminary Testing of the Finger Prototype

After the simulation program was validated, it was used to assess the level of performance of the current model finger by comparing the actual values of specific parameters to the ideal theoretical values. The parameters that were tested in the current finger were the position accuracy, repeatability, and joint speed.

The divergence between the actual position and the desired position was obtained by experimentation and the accuracy was calculated to be $\pm 5\text{mm}$ (Fig.23).

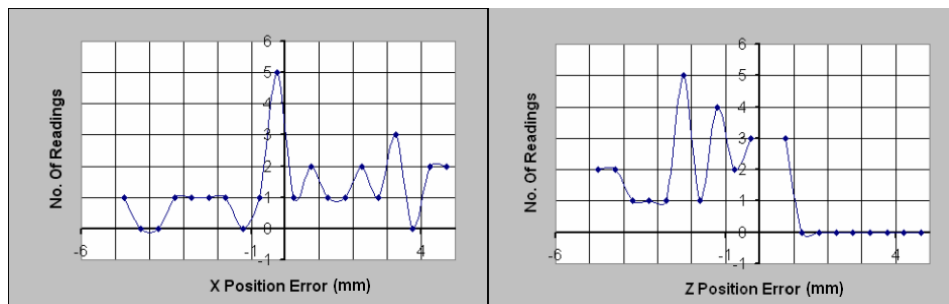


Figure 23 - X and Z Finger Tip Position Accuracy

A set of positions was selected and the fingertip was driven to these points from the initial calibrated position repeatedly. The variation between repeated positions was recorded and the difference between them was calculated and plotted (Fig. 24). The repeatability for x- and z-positions is $\pm 2\text{mm}$ whilst for the y-position it is $\pm 6\text{mm}$.

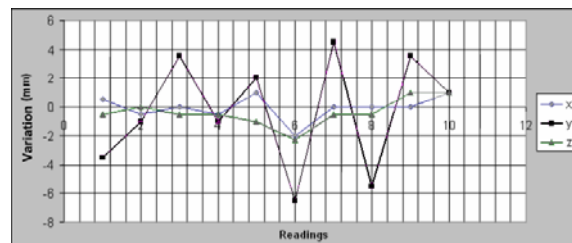


Figure 24 - Variation Obtained between Repeated Positions

In the present model the joint speeds have been limited to two degrees per second and the finger is currently able to apply a maximum force of approximately 5N.

7. Conclusion

In this work, we have developed, demonstrated and tested a new, four-joint, three-degree-of-freedom robot finger that is designed to form part of an anthropomorphic, dexterous robot hand. The design utilises actuators, transmission systems, and sensors that are integrated within the structure itself, in order to keep the design as compact as possible and to minimise the use of cables. Materials and components are selected to minimise both weight and cost of the finger. An innovative feature of the finger is the incorporation of an adjustable linkage between the PIP and DIP joints in the mechanical design, to enable the use of different coupling ratios between these two joint motions as required. Analyses of the kinematics and statics of the finger have been carried out, and used to develop versatile simulation programs that can be used to optimise design parameters of the finger. Current work involves the improvement of the mechanical systems of the finger to improve accuracy and force capability, further use of the simulation programs to obtain optimum values of link lengths and R_{DP} for specific fields of applications, and the implementation of a comprehensive control system for the finger based in part on the analysis described in this work.

References

- [1] S. Pheasant, "Bodyspace: Anthropometry, Ergonomics and Design", *Taylor and Francis (Printers) Ltd.*, 1986, pp 125-127.
- [2] M. Peters, K. Mackenzie, and P. Bryden, "Finger Length and Distal Finger Extent Patterns in Humans", *American Journal of Physical Anthropology*, **117**: 209-217 (2002).
- [3] M. A. Saliba, F. Farrugia, and A. Giordmaina, "A Compact Glove Input Device to Measure Human Hand, Wrist and Forearm Joint Positions for Teleoperation Applications", *Proceedings of the IEEE/APS International Conference on Mechatronics and Robotics (MechRob 2004)*, Aachen, Germany, September 2004.
- [4] J. Lin, Y. Wu, and T. S. Huang, "Modelling the Constraints of Human Hand Motion" *Proceedings of the Workshop on Human Motion, (HUMO 2000)*, Austin, Texas, December 2000.
- [5] M. A. Saliba, D. Camilleri and M. J. Farrugia, "Development of an Anthropomorphic Robot Hand and Wrist for Teleoperation Applications", *Proceedings of the IEEE International Conference on Information and Automation (ICIA 2005)*, Colombo, Sri Lanka, December 2005.
- [6] S. C. Jacobsen *et al.*, Design of the Utah/MIT Dexterous Hand", *Proceedings of the International Conference on Robotics and Automation (ICRA 1986)*, San Francisco, California, April 1986.
- [7] A. Caffaz and G. Cannata, "The Design and Development of the DIST-hand Dexterous Gripper, *Proceedings of the International Conference on Robotics and Automation (ICRA 1986)*, Leuven, Belgium, May 1998.
- [8] H. Kawasaki, H. Shimomura, and Y. Shimizu, "Educational-industrial Complex Development of an Anthropomorphic Robot Hand 'Gifu Hand' ", *Advanced Robotics*, Vol. 15, No. 3, pp 357-363 (2001).
- [9] S. Schulz, C. Pylatiuk, and G. Bretthauer, " A New Ultralight Anthropomorphic Hand", *Proceedings of the International Conference on Robotics and Automation (ICRA 2001)*, Seoul, Korea, May 2001.
- [10] Lotti, F., and Vassura, G., "A Novel Approach to Mechanical Design of Articulated Fingers for Robotic Hands," In *Proceedings of the 2002 IEEE/RSJ Intl. Conference on Intelligent Robots and Systems, Lausanne, Switzerland October 2002*.
- [11] Yamano, I., Takemura, K., and Maeno, T., "Development of a Robot Finger for a Five-Fingered Hand using Ultrasonic Motors" In *Proceedings of the 2003 IEEE/RSJ Intl. Conference on Intelligent Robots and Systems, Las Vegas, Nevada, October 2003*.
- [12] H. Liu *et al.*, "The Compact Multisensory HIT/DLR Hand", *Proceedings of the IEEE/APS International Conference on Mechatronics and Robotics (MechRob 2004)*, Aachen, Germany, September 2004.
- [13] J. Butterfass, M. Grebenstein, H. Liu, and G. Hirzinger, "DLR-Hand II: Next Generation of a Dexterous Robot Hand", *Proceedings of the International Conference on Robotics and Automation (ICRA 2001)*, Seoul, Korea, May 2001.
- [14] Maxon Motors ag "High Precision Drives and Systems Catalogue 04/05".

Nathaniel Mifsud received his Bachelors degree in Mechanical Engineering from the University of Malta in 2005. He was awarded second place from The Institution of Engineering Designers for the "Most Innovative Design" mechanical engineering project. Currently he is working with STMicroelectronics Malta as a process engineer in an area related to surface mount technology.

Anne Marie Grech received her Bachelors degree with first class honours in Mechanical Engineering from the University of Malta in 2004. She has been working as R&D Engineer in the CAE Team, Corporate Packaging and Automation group of STMicroelectronics since 2004. Currently she is carrying out research in reliability modelling for advanced IC packages.

Michael A. Saliba received his Bachelors degree in Mechanical Engineering from the University of Malta in 1986. Between 1986 and 1989 he worked as a Development Engineer for Air Malta Co. Ltd., and in 1989 moved to Canada where he obtained his M.A.Sc. degree in Mechanical Engineering and Ph.D. degree in Physics from the University of British Columbia in Vancouver, in 1991 and 1998 respectively. He was a Canadian Commonwealth scholar from 1989 to 1991 and a Westcott Memorial Fellow from 1996 to 1997. He was appointed lecturer in the Department of Manufacturing Engineering at the University of Malta in 1998, and senior lecturer in 2003, and he teaches and conducts research in Robotics and in Industrial Automation in the Faculty of Engineering at the University. His research interests include robotic grasping and handling, teleoperation, and industrial automation, and he is the author or co-author of various scientific papers in these areas. He is a licensed engineer, and a member of the ASME, IEEE, APS, and CoE (Malta).

Simon G. Fabri received the Electrical Engineering degree from the University of Malta in 1989, and the MSc and PhD degrees in Control Systems from the University of Sheffield, U.K. in 1994 and 1999 respectively. From 1989 to 1991, he was employed as a Test and Product Engineer with SGS-Thomson Microelectronics, Malta. In 1992 he was appointed academic staff member of the Faculty of Engineering at the University of Malta, where he currently holds the position of senior lecturer in Control Systems with the Department of Electrical Power and Control Engineering. His research interests include adaptive and intelligent control, neural networks, nonlinear control, robot control, stochastic control and biomedical engineering. He has published several articles in various conference proceedings and journals, and regularly acts as an article reviewer for the IEEE Transactions on Neural Networks, the IEE Proceedings, Automatica and various international conferences. He is currently chairing the Technical Programme Committee of the 3rd IEE International Conference on Advances in Medical, Signal and Information Processing. He is an Associate Editor of the *International Journal of Systems Science* and co-author of the Springer-Verlag book, *Functional Adaptive Control: An intelligent systems approach*.